Insight into the dynamics of ferrohydrodynamic (FHD) and magnetohydrodynamic (MHD) nanofluids inside a hexagonal cavity in the presence of a non-uniform magnetic field

M. Ghalambaz[a,b,*], M. Sabour[c], S. Sazgara[d], I. Pop[e], R. Trâmbiţaş[e]

[a] Department for Management of Science and Technology Development, Ton Duc Thang University, Ho Chi Minh City, Vietnam
[b] Faculty of Applied Sciences, Ton Duc Thang University, Ho Chi Minh City, Vietnam
[c] Young Researchers and Elite Club, Ahvaz Branch, Islamic Azad University, Ahvaz, Iran
[d] Mechnaical Engineering Department, Dezful Branch, Islamic Azad University, Dezful, Iran
[e] Faculty of Mathematics and Computer Science, Babeş-Bolyai University, 400084 Cluj-Napoca, Romania

ABSTRACT

The ferrohydrodynamic (FHD) and magnetohydrodynamic (MHD) are two important effects of a magnetic field in a liquid. FHD is the results of Kelvin force while MHD is the effect of a magnetic field due to Lorentz force. The present study aimed to evaluate the heat and mass transfer behavior of nanofluids inside a hexagonal enclosure in the presence of a non-uniform magnetic field considering the effects of Ferro-hydrodynamic (FHD) and Magneto-hydrodynamic (MHD). First, the concentration gradient of nanoparticles was captured due to the nanoscale forces. Then, the governing equations, including the continuity of nanofluid and nanoparticles, and momentum for vertical and horizontal direction were introduced, along with energy equation. Besides, the practical boundary condition of zero mass flux in nanoparticles at the walls was employed. Further, the governing equations were transformed into their non-dimensional form and solved numerically by the Finite Element Method (FEM). Furthermore, a systematic grid check was performed, and the results were compared with those of previous studies. Increasing magnetic number (Mnf) results in an increase in the heat and mass transfer rate. Increasing Lorentz force, in the form of Hartmann number (Ha) leads to a decrease in the rate of heat and mass transfer.

1. Introduction

During the recent years, the nanofluid has become an inseparable part of the natural, forced, and mixed convection heat transfer related to industries. Dispersing a certain volume fraction of nanoparticles in a base fluid can improve the rate of the base fluid heat transfer, as well as the performance and efficiency of industrial systems. However, there are some cases in natural convection heat transfer in which the synthesized nanofluid fails to improve, and deteriorates the heat transfer rate compare to the base fluid.

Elements such as the shape, material and particle size, basic fluid type and fluid operation temperature play a pivotal role in determining the value of improving and attenuating the heat transfer rate [1]. Considering the mentioned elements and assuming to achieve the enhanced heat transfer rate via nanoparticles, maintaining the status and continuing their proper circulation inside the enclosure is regarded as one of the most important issues in the related industries. Industrial

equipment, along with the included systems of the nanofluid can change the rate of heat and mass transfer in nanoparticles such as uniform and local magnetic fields, which can create magnetic nanoparticles or the nanofluid permanently and periodically.

The nanofluid flow can be converted into a Ferro-hydrodynamic (FHD) with steady magnetism and a Magneto-hydrodynamic (MHD) with a temporary dynamic property, or a combination of Ferro-hydrodynamic and Magneto-hydrodynamics. Thus, the circulation of the nanofluid (base fluid + nanoparticles) is not just a function of the heat and mass transfer mechanisms, while the presence of magnetic fields can affect the nanofluid movements [2,3].

Buongiorno [4] presented a non-homogeneous model for the nanofluid and evaluated the effects of motion and sliding mechanisms of nanoparticles by considering the nanofluid as a non-homogeneous mixture. Among the proposed mechanisms, just Brownian arising from random movements of nanoparticles and Thermophoresis diffusions as the motion of nanoparticles due to thermal gradients played a

---

*Corresponding author at: Ton Duc Thang University, Ho Chi Minh City, Vietnam.
 E-mail address: mohammad.ghalambaz@tdtu.edu.vn (M. Ghalambaz).

Nomenclature

B	Magnetic induction (flux density) (T)
C	Dimensional concentration of nanoparticles
C_p	Specific heat in constant pressure $(\mathrm{J\,kg^{-1o}\,K^{-1}})$
D_B	Brownian diffusion coefficients $(\mathrm{m^2\,s^{-1}})$
D_T	Thermophoretic diffusion coefficient $(\mathrm{m^2\,s^{-1}})$
Ec	Eckert number
g	Gravitational force $(\mathrm{m\,s^{-2}})$
H	Magnetic field strength $(\mathrm{A\,m^{-1}})$
Ha	Hartmann number
I	Magnetic field strength at a source $(\mathrm{A\,m^{-1}})$
k	Thermal conductivity $(\mathrm{W\,m^{-1o}\,K^{-1}})$
K'	Constant parameter
L	Length of enclosure (m)
Le	Lewis number
M^*	Dimensional magnetization $(\mathrm{A\,m^{-1}})$
Mnf	Magnetic number
N_b	Brownian motion parameter
Nc	Thermal conductivity parameter
N_r	Buoyancy ratio parameter
N_t	Thermophoresis motion parameter
Nu	Nusselt number
$N\nu$	Dynamic viscosity parameter
P	Pressure (Pa)
Pr	Prandtl number
Ra	Rayleigh number
Sh	Sherwood number
T	Dimensional temperature $(^\circ K)$
T'_c	Curie temperature
u	Horizontal component of velocity $(\mathrm{m\,s^{-1}})$
	Vertical component of velocity $(\mathrm{m\,s^{-1}})$
x	Cartesian coordinate in horizontal direction (m)
y	Cartesian coordinate in vertical direction (m)

Greek symbols

α	Thermal diffusivity $(\mathrm{m^2\,s^{-1}})$
β	Volumetric expansion coefficient $^\circ K^{-1}$
δ	Angle of magnetic field
ε_1	Temperature number
ε_2	Curie temperature number
ϕ	Non-dimensional concentration of nanoparticles
μ	Dynamic viscosity $(kg\,\mathrm{m^{-1}\,s^{-1}})$
μ_0	Magnetic permeability of vacuum $(\mathrm{T\,M\,A^{-1}})$
θ	Non-dimensional temperature
ρ	Density $(\mathrm{kg\,m^{-3}})$
σ	Electrical conductivity $(\mathrm{s\,m^{-1}})$

Subscripts

Avg	Average value
bf	Base fluid
c	Cold
h	Hot
nf	Nanofluid
p	Particles
0	Reference

Superscripts

$*$	Variables in dimensional form

significant role in the nanoparticle motion. In another study, Buongiorno et al. [5] measured the thermal conductivity coefficient of 8 samples of nanofluids in 30 different regions of the world by using hot wire, steady flow, and optical laboratory methods. Based on the results, the thermal conductivity coefficient is a linear function of the volume fraction of nanoparticles. Besides, the rate measured by the three methods was different.

Celli [6] used the non-\homogeneous method (Buongiorno's model) to examine the heat transfer of the natural convection for alumina/water nanofluid with the nanoparticle diameter of 10 nm inside an enclosure, as well as the mechanism of mass transfer in nanoparticles, including Brownian motion and thermophoresis effects in the utilized nanofluid model. The results indicated that the distribution of nanoparticles has a particular sensitivity to low Rayleigh numbers. Wakif et al. [7] employed a generalized Buongiorno's mathematical model to address the effect of alumina nanoparticle's on the transport of nanoparticles in the presence of a magnetic field. The Oberbeck-Boussinesq approximation was utilized to model the buoyancy forces and simplified Maxwell's equations was adopted for the magnetic field. Behseresht et al. [8] utilized a practical range of non-dimensional parameters for thermophoresis and Brownian motion and investigated the natural convection flow of nanofluids over a hot cone. In a very recent study, Mahian et al. [9,10] analyzed the modeling approaches and physical mechanisms of nanofluid heat transfer. Other aspects of heat transfer of nanofluids such as radiation and damped thermal flux [11], Hall effects with variable dynamic viscosity and density [12], and chemically reactions [13] are also addressed.

Nowadays, magnet materials are classified in a hard and soft mode and are used in different aspects of sciences and technologies [14]. For example, a permanent magnet material can separate blood red cells in the form of a magnetic device in medical applications [15]. For example, Tzirtzilakis and Xenus [16] studied the biomagnetic (ferrohydrodynamics and magnetohydrodynamics) fluid flow in the absence of heat transfer equations and considered biomagnetic blood as a Newtonian and homogeneous fluid, which was affected by electric and magnetic fields. Based on the results, the presence of the magnetic field significantly influenced the streamline and the velocity of the fluid (blood).

As mentioned, MHD flows are concerned with the effect of a magnetic field on the dynamic of a fluid due to the Lorentz force. MHD flow and heat transfer have been studied in many of literature works. Al-Najem et al. [17] emphasized the effect of the presence of a uniform magnetic field on the natural convection heat transfer inside a tilted square enclosure for different values of Grashof and Hartmann numbers. The results indicated that the presence of a uniform magnetic field at smaller deviation angles (for tilted enclosure) and higher values of Grashof number play a significant role in the laminar flow convection and heat transfer rate. Selimefendigil et al. [18] focused on the effect of the presence of a strong and angular magnetic field on the natural convection heat transfer of the copper-oxide-water nanofluid inside an enclosure with movable led. They concluded that the angle of the magnetic field significantly affected the natural convection heat transfer, and the presence of the uniform magnetic field reduced the heat transfer inside the enclosure.

Ghalambaz et al. [19] evaluated the effects of a uniform magnetic field and the tilted angle of the enclosure on the melting behavior of an electrical conductive PCM (phase change material). Based on the results, any increase in the Hartmann number and the angle of the enclosure leads to a decrease in the melting ratio. Chamkha et al. [20] evaluated the effect of a uniform magnetic field on the entropy generation in a cavity filled with copper/water nanofluid and indicated that magnetic field. They found that the magnetic field can reduce the entropy generation. There are also some recent studies that addressed the MHD natural convection flow of nanofluids using single phase

model.

Ma et al. [21] explored the effect of a uniform inclined magnetic field on the natural convection flow and heat transfer of CuO/water nanofluid in a U-shaped cavity. The outcomes show that the increase of the magnetic field intensity reduces the heat transfer rate in the cavity. Dogonchi et al. [22] investigated the effect of a uniform magnetic field on the natural convection heat transfer of CuO/water nanofluid in a horizontal semi-cylinder. The outcomes in agreement with the study of Ma et al. [21] confirms the reduction of heat transfer by the increase of the intensity of the magnetic field. Sivaraj and Sheremet [23] analyzed the effect of an inclined magnetic field on the natural convection flow, heat transfer, and entropy generation of Fe_3O_4/water nanofluid in a cavity. The results show that the magnetic field suppresses the entropy generation and natural convection heat transfer. They also found that the inclination angle of the magnetic field can act as a controlling parameter for control of heat transfer in the cavity.

The ferrohydrodynamics effect is results of Kelvin force, in which, a magnetic field affects a magnetized liquid. Considering FDH effects, Sheikholeslami and Domiri-Ganji [3] addressed the Ferro-hydrodynamic c effects on the natural convection heat transfer rate of the Water-CuO nanofluid using a homogeneous model of nanofluids. Based on the results, the Nusselt number improves by increasing the Rayleigh number and volume fraction of nanoparticles. In another study, Sheikholeslami et al. [24] evaluated forced convection heat transfer of the biomagnetic fluid by considering the iron oxide/water nanofluid as a homogeneous and single-phase fluid and indicated that the effect of Magnetic number on the forced heat transfer rate is more considerable in the high values of Reynold number. Further, an increase in Hartmann number leads to a reduction in the heat transfer rate while increasing the magnetic and Reynolds numbers enhances the heat transfer rate.

Aminfar et al. [25] probed convection heat transfer of water-Fe_2O_3 nanofluid inside of a vertical 3D duct and utilized finite volume method (FVM). Based on the results, magnetic fields arising from negative axial gradients and uniform transverse profiles improved heat transfer rate although those exposed to positive gradient profile deteriorated heat transfer rate. Rostami-Dibavar et al. [26] examined FHD and MHD effects on the melting and solidification of a homogenous nanofluid through finite element method (FEM) and found that an increase in magnetic number results in reducing the required time for melting and solidifying the phase changing materials, while an increase in Hartmann number leads to an increase in the required time.

Several recent studies addressed the non-uniform distribution of nanoparticles, due to Brownian motion and thermophoresis forces, in natural convection flow of nanofluids in enclosure cavities. Sheremet and Pop [27] evaluated a porous medium filled with nanofluid using Buongiorno's mathematical and considering the effect of thermophoresis and Brownian motion, and accordingly non-dimensional numbers of Lewis and Rayleigh on the heat and mass transfer of nanofluids were determined. Based on the results, the thermophoresis force increased, the parameters such as Brownian motion decreased, and Lewis and Rayleigh numbers increased the non-homogeneous distribution of the nanoparticles in the porous enclosure. Khan and Pop [28] investigated the flow of the boundary layer of a nanofluid passing over a straight plate and indicated that the Nusselt number decreases by decreasing each of the mentioned non-dimensional parameters. Hashim et al. [29] addressed the natural convection of nanofluids in a wavy wall cavity. Stanina et al. [30] focused on natural convection heat transfer of non-homogenous Water-CuO nanofluid inside a square enclosure and simulated the mentioned problem as time-dependent for different volume fractions of nanoparticles. Ho et al. [31] examined the natural heat transfer in a square enclosure, both numerically and experimentally. The results indicated that the thermophoresis force has the most substantial contribution to the distribution of volume fraction in nanoparticles. Thus, dispensing the nanoparticle volume fraction failed to be compiled from the distribution of the water fluid phase.

By considering the above literature, the non-homogeneous models
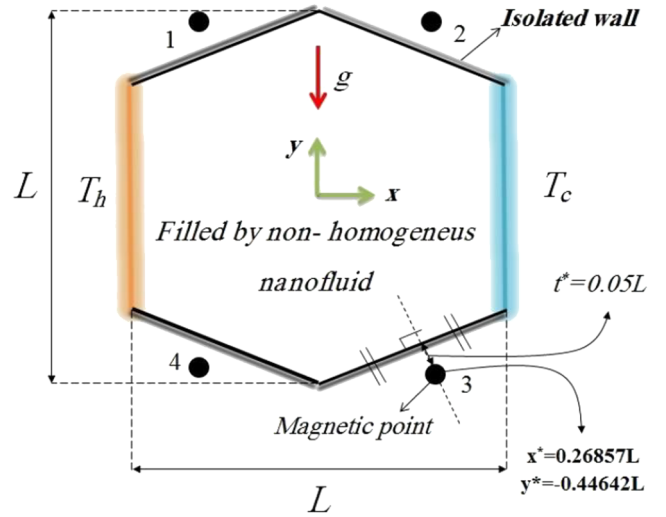

Fig. 1. A schematic diagram of the physical model.

of nanofluids and MHD effects have been addressed in some of the recent studies. However, the FHD effects on the non-uniform distribution of nanoparticles is a new subject. The present study aims to address the effect of a variable magnetic field, incorporating MHD and FHD, on the nanoparticle distribution, flow, and heat transfer of nanofluids.

2. Physical and mathematical model'

As shown in Fig. 1, a hexagonal enclosure, honeycomb, filled with a nanofluid with dimensions of equivalent L is exposed to a non-uniform magnetic field which the source can be placed at each of the locations (1–4). In addition, each source is located with a vertical distance of 0.05 L from each tilted wall. Further, the nanofluid is considered as non-homogeneous, which allows for the slip between the nanoparticles and the base fluid. Thus, the volume fraction of nanoparticles in the cavity can be changed. The nanofluid is assumed to be Newtonian, incompressible, and steady, along with the use of the Boussinesq's approximation within the hexagonal enclosure. Furthermore, the local magnetic field induces the effects of Ferrohydrodynamic (FHD) and Magnetohydrodynamic (MHD) into non-homogeneous nanofluid. Regarding the governing boundary conditions, every four tilted walls are assumed as insulated, and no heat and mass transfer is passed from these walls. The left and right vertical walls are isothermal at a higher temperature (T_h) and lower temperature (T_c), respectively.

Governing equations of natural convection heat transfer of the non-homogeneous nanofluid in the presence of a local magnetic field by considering the effects of Ferrohidrodynamic (FHD) and Magnetohydrodynamic (MHD) can be introduced as continuity equations for the mixture, momentum equations in the horizontal and vertical direction, as well as the energy equation for nanofluid and continuity equation for nanoparticles. The dimensional form of these equations is as follows [3,30]:

$$\frac{\partial u^*}{\partial x^*} + \frac{\partial v^*}{\partial y^*} = 0 \tag{1}$$

$$\rho_{nf}\left(u^*\frac{\partial u^*}{\partial x^*} + v^*\frac{\partial u^*}{\partial y^*}\right)$$
$$= -\frac{\partial p^*}{\partial x^*} + \mu_{nf}\left(\frac{\partial^2 u^*}{\partial x^{*2}} + \frac{\partial^2 u^*}{\partial y^{*2}}\right) + \mu_0 M^*\frac{\partial H^*}{\partial x^*} - \sigma_{nf}B_y^{*2}u^* + \sigma_{nf}B_x^*B_y^*v^*$$

$$\tag{2}$$

$$\rho_{nf}\left(u^*\frac{\partial v^*}{\partial x^*} + v^*\frac{\partial v^*}{\partial y^*}\right)$$

$$= -\frac{\partial p^*}{\partial y^*} + \mu_0 M^*\frac{\partial H^*}{\partial y^*} - \sigma_{nf}B_x^{*2}v^* + \sigma_{nf}B_x^*B_y^*u^* + \mu_{nf}$$

$$\left(\frac{\partial^2 v^*}{\partial x^{*2}} + \frac{\partial^2 v^*}{\partial y^{*2}}\right) + \rho_{nf}\vec{g}$$

(3)

$$(\rho c_p)_{nf}\left(u^*\frac{\partial T}{\partial x^*} + v^*\frac{\partial T}{\partial y^*}\right)$$

$$= k_{nf}\left(\frac{\partial^2 T}{\partial x^{*2}} + \frac{\partial^2 T}{\partial y^{*2}}\right) + (\rho c_p)_p\left(D_B\left(\frac{\partial C}{\partial x^*}\frac{\partial T}{\partial x^*} + \frac{\partial C}{\partial y^*}\frac{\partial T}{\partial y^*}\right)\right.$$

$$\left. + \frac{D_T}{T}\left(\left(\frac{\partial T}{\partial x^*}\right)^2 + \left(\frac{\partial T}{\partial y^*}\right)^2\right)\right) + \sigma_{nf}(u^*B_y^* - v^*B_x^*)^2 - \mu_0$$

$$T\frac{\partial M^*}{\partial T}\left(u^*\frac{\partial H^*}{\partial x^*} + v^*\frac{\partial H^*}{\partial y^*}\right)$$

(4)

$$u^*\frac{\partial C}{\partial x^*} + v^*\frac{\partial C}{\partial y^*} = D_B\left(\frac{\partial^2 C}{\partial x^{*2}} + \frac{\partial^2 C}{\partial y^{*2}}\right) + \frac{D_T}{T_c}\left(\frac{\partial^2 T}{\partial x^{*2}} + \frac{\partial^2 T}{\partial y^{*2}}\right)$$

(5)

where,

$$M^* = K'H^*(T_c' - T)$$

(6)

FHD and MHD effects are considered in the form of Kelvin and Lorentz forces in Eqs. (2) and (3). The term $\mu_0 M^*\frac{\partial H^*}{\partial x^*}$ (or in the vertical direction) represents FHD effects and terms $\sigma_{nf}B_y^{*2}u^* + \sigma_{nf}B_x^*B_y^*v^*$ (or in the vertical direction) indicate the MHD effects. Besides, ρ_{nf}, P^*, M^*, σ_{nf}, B^*, μ_{nf} in momentum equations indicate the nanofluid density, dimensional pressure, dimensional Magnetization, electrical conductivity, dimensional magnetic induction, and dynamic viscosity of

nanofluid, respectively. Further, $D_B\left(\frac{\partial^2 C}{\partial x^{*2}} + \frac{\partial^2 C}{\partial y^{*2}}\right)$ and $\frac{D_T}{T_c}\left(\frac{\partial^2 T}{\partial x^{*2}} + \frac{\partial^2 T}{\partial y^{*2}}\right)$ show the dispersion of nanoparticles by Brownian motion (random motion of nanoparticles) and Thermophoresis force (motion of nanoparticles affecting thermal gradients), as observed in Eq. (1), where x^* and y^* represent Cartesian coordinates (m), u^* and v^* are the velocity components, along with horizontal and vertical directions (ms^{-1}).C is considered as the concentration of nanoparticles, D_B and D_T are Brownian and Thermophoresis diffusion coefficients (m^2s^{-1}), and T is regarded as dimensional temperature (K). Besides, FHD and MHD effects in energy equation are considered, where $\mu_0 T\frac{\partial M}{\partial T}\left(u^*\frac{\partial H^*}{\partial x^*} + v^*\frac{\partial H^*}{\partial y^*}\right)$ maintains the magneto-caloric effects and is derived from FHD. On the other hand, $\sigma_{nf}(u^*B_y^* - v^*B_x^*)^2$ in Eq. (5) is the result of the effects of Joule heating and derived from MHD [3,24].

Eq. (5) indicates the magnetic field strength (H^*) in the dimensional form, where, a magnetic source is located in one of the four positions (Fig. 1). Thus, it is positioned at $-d_2^*$ and $-d_1^*$ from the origin of horizontal and vertical axes [32]:

$$H^*(x^*, y^*) = \frac{I}{2\pi r^*}\delta, r^* = \sqrt{(x^* + d_2^*)^2 + (y^* + d_1^*)^2}, \delta$$

$$= \frac{y^* + d_1^*}{r^*}i - \frac{x^* + d_2^*}{r^*}j$$

$$H_x^*(x^*, y^*) = \frac{I}{2\pi}\frac{y^* + d_1^*}{r^{*2}}, H_y^*(x^*, y^*) = -\frac{I}{2\pi}\frac{x^* + d_2^*}{r^{*2}}$$

$$H^*(x^*, y^*) = \sqrt{H_x^{*2} + H_y^{*2}}$$

(7)

where I and δ are internal strength (A/m) and angle of the magnetic field, respectively. As shown in Fig. 1, the boundary conditions associated with the physical schematic are described for fluid flow temperature and the mass transfer in the form of mathematical relations

Table 1
The dimensional form of the boundary conditions in the present study.

(8)

$$u^*(x^*, y^*) = v^*(x^*, y^*) = 0, \frac{\partial C}{\partial n^*} = \frac{\partial T}{\partial n^*}\bigg|_{(x^*,y^*)} = 0,$$
$$-0.5L \leq x^* \leq 0, y^* = -0.4x^* - 0.5L.$$

$$u^*(-0.5L, y^*) = v^*(-0.5L, y^*) = 0, T(-0.5L, y^*) = T_h,$$
$$N_b\frac{\partial C}{\partial x^*}\bigg|_{(-0.5L,y^*)} + N_t\frac{\partial \theta}{\partial x^*}\bigg|_{(-0.5L,y^*)} = 0, -0.3L \leq y^* \leq 0.3L$$

$$u^*(x^*, y^*) = v^*(x^*, y^*) = 0, \frac{\partial C}{\partial n^*} = \frac{\partial T}{\partial n^*}\bigg|_{(x^*,y^*)} = 0,$$
$$-0.5L \leq x^* \leq 0, y^* = 0.4x^* + 0.5L$$

$$u^*(x^*, y^*) = v^*(x^*, y^*) = 0, \frac{\partial C}{\partial n^*} = \frac{\partial T}{\partial n^*}\bigg|_{(x^*,y^*)} = 0,$$
$$0 \leq x^* \leq 0.5L, y^* = -0.4x^* + 0.5L$$

$$u^*(0.5L, y^*) = v^*(0.5L, y^*) = 0, T(0.5L, y^*) = T_c,$$
$$N_b\frac{\partial C}{\partial n^*}\bigg|_{(0.5L,y^*)} + N_t\frac{\partial T}{\partial n^*}\bigg|_{(0.5L,y^*)} = 0, -0.3L \leq y^* \leq 0.3L$$

$$u^*(x^*, y^*) = v^*(x^*, y^*) = 0, \frac{\partial C}{\partial n^*} = \frac{\partial T}{\partial n^*}\bigg|_{(x^*,y^*)} = 0,$$
$$0 \leq x^* \leq 0.5L, y^* = 0.4x^* - 0.5L$$

where n is normal to the surface (Table 1).

In order to generalize the solution, Eqs. (1)–(5) and related boundary conditions (Eq. (8)) are transformed to their non-dimensional form. In order to obtain the non-dimensional form of the mentioned equations, the following non-dimensional parameters are introduced as follows:

$$x = \frac{x^*}{L}, \, y = \frac{y^*}{L}, \, u = \frac{u^*L}{\alpha_{bf}}, \, v = \frac{v^*L}{\alpha_{bf}},$$

$$P = \frac{P^*L^2}{\rho_{bf}\alpha_{bf}^2}, \, \theta = \frac{T - T_c}{T_h - T_c}, \, \phi = \frac{C}{\phi_0}, \, H = \frac{H^*(x^*, y^*)}{H_0^*} \quad (9)$$

By utilizing Eq. (9), the final and non-dimensional form of Eqs. (1)–(5) and (7) is obtained in the form of Eqs. ((10)–(15)):

Continuity of the mixture:

$$\frac{\partial u}{\partial x} + \frac{\partial v}{\partial y} = 0 \quad (10)$$

Momentum in x and y:

$$u\frac{\partial u}{\partial x} + v\frac{\partial u}{\partial y}$$
$$= -\frac{\rho_{bf}}{\rho_{nf}}\frac{\partial p}{\partial x} + \frac{\rho_{bf}}{\rho_{nf}}MnfH\frac{\partial H}{\partial x}(\varepsilon_2 - \varepsilon_1 - \theta) + \frac{\sigma_{nf}}{\sigma_{bf}}\frac{\rho_{bf}}{\rho_{nf}}H$$
$$a^2\Pr(H_xH_yv - H_y^2u) + \frac{\rho_{bf}}{\rho_{nf}}\frac{\mu_{nf}}{\mu_{bf}}\Pr\left(\frac{\partial^2 u}{\partial x^2} + \frac{\partial^2 u}{\partial y^2}\right) \quad (11)$$

$$u\frac{\partial v}{\partial x} + v\frac{\partial v}{\partial y}$$
$$= -\frac{\rho_{bf}}{\rho_{nf}}\frac{\partial p}{\partial y} + \frac{\rho_{bf}}{\rho_{nf}}MnfH\frac{\partial H}{\partial y}(\varepsilon_2 - \varepsilon_1 - \theta) + \frac{\sigma_{nf}}{\sigma_{bf}}\frac{\rho_{bf}}{\rho_{nf}}Ha^2$$
$$\Pr(H_xH_yu - H_x^2v) + \frac{\rho_{bf}}{\rho_{nf}}\frac{\mu_{nf}}{\mu_{bf}}\Pr\left(\frac{\partial^2 v}{\partial x^2} + \frac{\partial^2 v}{\partial y^2}\right) + \frac{\rho_{bf}}{\rho_{nf}}Ra\Pr N_r$$
$$(1 - \phi) + \frac{\beta_{nf}}{\beta_{bf}}Ra\Pr(1 - \phi\phi_0)\theta \quad (12)$$

Energy equation:

$$u\frac{\partial \theta}{\partial x} + v\frac{\partial \theta}{\partial y}$$
$$= \frac{\alpha_{nf}}{\alpha_{bf}}\left(\frac{\partial^2\theta}{\partial x^2} + \frac{\partial^2\theta}{\partial y^2}\right) + N_b\left(\frac{\partial\phi}{\partial x}\frac{\partial\theta}{\partial x} + \frac{\partial\phi}{\partial y}\frac{\partial\theta}{\partial y}\right) + N_t$$
$$\left(\left(\frac{\partial\theta}{\partial x}\right)^2 + \left(\frac{\partial\theta}{\partial y}\right)^2\right) + \frac{\sigma_{nf}}{\sigma_{bf}}\frac{(\rho c_p)_{bf}}{(\rho c_p)_{nf}}Ha^2Ec(uH_y - vH_x)^2 + \frac{(\rho c_p)_{bf}}{(\rho c_p)_{nf}}EcMnf$$
$$H(\theta + \varepsilon_1)\left(u\frac{\partial H}{\partial x} + v\frac{\partial H}{\partial y}\right) \quad (13)$$

Continuity of the nanoparticles:

$$Le\left(u\frac{\partial \phi}{\partial x} + v\frac{\partial \phi}{\partial y}\right) = \frac{\partial^2\phi}{\partial x^2} + \frac{\partial^2\phi}{\partial y^2} + \frac{N_t}{N_b}\left(\frac{\partial^2\theta}{\partial x^2} + \frac{\partial^2\theta}{\partial y^2}\right) \quad (14)$$

Magnetic field:

$$H_x(x, y) = \frac{H_x^*(x^*, y^*)}{H_0^*(-d_2^*, 0)} = \frac{d_1(y + d_1)}{r^2},$$
$$H_y(x, y) = \frac{H_y^*(x^*, y^*)}{H_0^*(-d_2^*, 0)} = -\frac{d_1(x + d_2)}{r^2} \quad (15)$$

where,

$$H_0^*(-d_2^*, 0) = \frac{I}{2\pi}\frac{1}{d_1^*} \quad (16)$$

In the above equations, the dimensionless numbers of Lewis (Le), magnetic (Mnf), Curie temperature (ε_2), temperature (ε_1), Hartmann (Ha), Prandtl (Pr), Rayleigh (Ra) and Eckert (Ec) as well as dimensionless parameters such as Buoyancy ratio (Nr), Brownian (N_b)

and Thermophoresis (N_t) motions are defined as follows [24,33]:

$$Le = \frac{\alpha_{bf}}{D_B}, \quad Mnf = \frac{\mu_0 H_0^2 k'\Delta TI^2}{\mu_{bf}\alpha_{bf}}, \quad \varepsilon_2 = \frac{T_c'}{\Delta T}, \quad \varepsilon_1 = \frac{T_c}{\Delta T}, \quad Ha = L\mu_0H_0\sqrt{\frac{\sigma_{bf}}{\mu_{bf}}},$$

$$Pr = \frac{\upsilon_{bf}}{\alpha_{bf}},$$

$$Ra = \frac{g\beta_{bf}\Delta TI^3}{\alpha_{bf}\upsilon_{bf}}, \quad Ec = \frac{\mu_{bf}\alpha_{bf}}{(\rho c_p)_{bf}\Delta TI^2}, \quad N_r = \frac{(\rho_p - \rho_{bf})\phi_0}{\beta_{bf}\Delta T\rho_{bf}}, \quad N_b = \frac{(\rho c_p)_p D_B\phi_0}{(\rho c_p)_{nf}\alpha_{bf}},$$

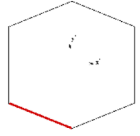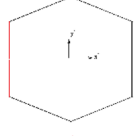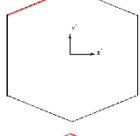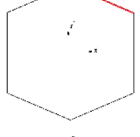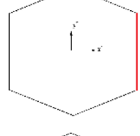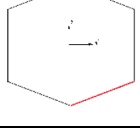$$N_t = \frac{(\rho c_p)_p(T_h - T_c)D_T}{(\rho c_p)_{nf}\alpha_{bf}T} \quad (17)$$

Some thermo-physical relations are required for evaluating the dynamic viscosity ratio of the nanofluid to base fluid and the thermal conductivity ratio of nanofluid to base fluid. The following two equations can be utilized to evaluate the dynamic viscosity and thermal conductivity of nanofluids [34].

$$\frac{\mu_{nf}}{\mu_{bf}} = 1 + Nv\phi_0$$
$$\frac{k_{nf}}{k_{bf}} = 1 + Nc\phi_0 \quad (18)$$

where the symbols Nc and Nv are two non-dimensional numbers, called thermal conductivity and dynamic viscosity numbers. The numbers depend on the shape, size, type of nanoparticles, type of base fluid, and fluid operating temperature, which can be obtained for a nanofluid sample by using experimental data [35]. The above linear relations are adopted as the conclusion of the benchmark experimental studies of [5,36]. As shown in Table 2, a set of boundary conditions are transmitted in their non-dimensional form Table 3.

In the next stage, the average Nusselt is introduced at the hot wall in order to determine the exact amount of heat transfer on the hot wall. It

Table 2
The non-dimensional form of the boundary conditions.

$u(x, y) = v(x, y) = 0, \frac{\partial\phi}{\partial n} = \frac{\partial\theta}{\partial n}\big|_{(x,y)} = 0,$ $-0.5 \leq x \leq 0, y = -0.4x - 0.5.$	(19)
$u(-0.5, y) = v(-0.5, y) = 0, \theta(-0.5, y) = 1,$ $N_b\frac{\partial\phi}{\partial x}\big|_{(-0.5,y)} + N_t\frac{\partial\theta}{\partial x}\big|_{(-0.5,y)} = 0, -0.3 \leq y \leq 0.3.$	
$u(x, y) = v(x, y) = 0, \frac{\partial\phi}{\partial n} = \frac{\partial\theta}{\partial n}\big|_{(x,y)} = 0,$ $-0.5 \leq x \leq 0, y = 0.4x + 0.5.$	
$u(x, y) = v(x, y) = 0, \frac{\partial\phi}{\partial n} = \frac{\partial\theta}{\partial n}\big|_{(x,y)} = 0,$ $0 \leq x \leq 0.5, y = -0.4x + 0.5.$	
$u(0.5, y) = v(0.5, y) = 0, \theta(0.5, y) = 0,$ $N_b\frac{\partial\phi}{\partial n}\big|_{(0.5,y)} + N_t\frac{\partial\theta}{\partial n}\big|_{(0.5,y)} = 0, -0.3 \leq y \leq 0.3$	
$u(x, y) = v(x, y) = 0, \frac{\partial\phi}{\partial n} = \frac{\partial\theta}{\partial n}\big|_{(x,y)} = 0,$ $0 \leq x \leq 0.5, y = 0.4x - 0.5.$	

Table 3

Independence evaluation of Nusselt number, Sherwood number, and average velocity values for the computing grid size for $Nr = 5$, $\phi_0 = 2\%$, $N_b = 10^{-6}$, $N_t = 5 \times 10^{-7}$, $Nc = Nv = 7$, $Pr = 7$, $Ra = 10^4$ and $Le = 10^4$.

Grid size	Average Nusselt number (Nu_{avg})	Average Sherwood number (Sh_{avg})	Average Velocity (V)
4312	1.5763	0.6870	6.8568
6070	1.5760	0.6881	6.8632
7914	1.5758	0.6884	6.8648
9762	1.5759	0.6889	6.8656

is worth noting that the Sherwood number can be evaluated by using the boundary condition of the nanoparticle impermeability on the cold and hot walls.

$$Nu_{nf} = \int_{-0.3}^{0.3} -\frac{k_{nf}}{k_{bf}}\frac{\partial\theta}{\partial x}dy, \quad Sh_{nf} = \int_{-0.3}^{0.3} -\frac{N_t}{N_b}\frac{\partial\theta}{\partial x}dy \quad (20)$$

3. Numerical solution method and grid check

The problem including the partial differential equations (The equations for heat and mass transfer and the related boundary conditions) was written in the weak form, and then, the finite element method was employed to integrate the equations. Besides, an unstructured triangular grid form was selected to discretize the governing equations into a set of algebraic equations. A second-order accuracy scheme was utilized for the discretization of the momentum equations. Then, a linear discretization scheme was employed for the heat and nanoparticles continuity. The equations were considered as fully coupled, and the Newton method was utilized to solve the equations iteratively. Then, the calculations were repeated until the residuals decreased below 10^{-6}. More details about the numerical scheme of the present study are found in [37,38].

In order to utilize grid elements of this study as triangular, the calculations were repeated for four different grid sizes as indicated in Table 1. The values of non-dimensional average Nessult and Sherwood Numbers, along with average velocity were provided for mentioned grids with no magnetic field. As shown, regarding the case with the mesh size of 7914, the variations of the average Nusselt and Sherwood numbers, and the average velocity are very small with the order of 10^{-3}. Thus, this grid size is appropriate for obtaining the results. Hence, all of the results were provided by the computational grid size of 7914. Fig. 2 depicts the utilized grid for the calculations in the present study.

Following the method described in Shah et al. [39], the slope of linear variation of Grid size (x-axis) against the Nu_{avg}, Sh_{avg} and Average velocity are obtained as -7.64×10^{-8}, 3.29×10^{-7}, and 1.53×10^{-5}. As seen, the velocity profiles are the most sensitive variables to the grid size. This is mainly because of the velocity gradients next to the walls. The average Nusselt number is the less sensitive parameter to the grid size.

4. Validation

Before obtaining and displaying the results, the accuracy of the present code was checked against the amount in the previous studies. For this purpose, the computer code related to this study was validated with the number in two previous valid works. In the first step, a comparison between the present study and Celli work [6] was performed. As mentioned in the introduction section, Celli [6] used Buongiorno's model in a simple square enclosure with no magnetic field effects. Also, he used Brinkman and Maxwell relationships to determine the dynamic viscosity and the thermal conductivity ratios of the water-Al$_2$O$_3$ nanofluid, respectively. The equal values of non-dimensional dynamic viscosity (Nv) and thermal conductivity (Nc) parameters for Celli's work [6] were considered as 2.88 and 3.30, respectively. In the case of Water-Al$_2$O$_3$ with 1% volume fraction in nanoparticles, the results of the

present study were compared with those of Celli's work [6]. Then, the results were plotted in Fig. 3 for various values of Rayleigh number, as well as for the pure water with 0% nanoparticles. As shown in Fig. 3, the presence of nanoparticles, especially in high values of Rayleigh number, resulted in reducing the heat transfer rate. Further, the results are consistent with those of Celli [6].

In the second step, a comparison was performed between the results of the present study and those of Sathyamurthy and Chamkha [2]. In [2], the effect of the presence of a uniform magnetic field by its different angles was examined on the natural convection heat transfer rate. Furthermore, a melted metal was selected as an operating fluid with the non-dimensional Prandtl number $Pr = 0.054$. Among the given boundary conditions in the square enclosure, left and bottom walls are in the hot temperature, while the right and top walls are in the cold temperature. As illustrated in Fig. 4, variations of Hartmann number (Ha) and magnetic field angle (φ_0) in the two curves for local Nusselt number on the hot left wall are entirely consistent with the provided curves in the study of Sathiyamoorthy and Chamkha [2].

5. Results and discussion

The following range of non-dimensional parameters was adopted for presenting the results. The default values of Prandtl, Lewis, and Eckert numbers are fixed, which are equal to 7, 10^{+4} and 10^{-4}, respectively. Besides, the volume fraction of nanoparticles is applied to be 2%. In addition to evaluating Rayleigh number as the most important parameter in the natural convection heat transfer problems, other effective parameters such as the dynamic viscosity (Nv), thermal conductivity (Nc), buoyancy ratio (Nr), Brownian (Nb) and Thermophoresis motion (Nt) parameters, Hartmann (Ha) and magnetic numbers (Mnf) are summarized in Table 2.

Given the locality of the magnetic source, the most important question in this study can be related to the situation of the magnetic source around the enclosure. Thus, the values of the Nusselt and Sherwood numbers, as well as the nanofluid velocity, are given for the default values (D.V) of non-dimensional parameters (Table 5). Based on the results, the highest and lowest rate of heat and mass transfer occur in situation 2 and 3, respectively. However, the maximum and minimum values of the average velocity are related to situations 3 and 2, respectively. Hence, increasing the nanofluid velocity inside the enclosure does not necessarily mean an increase in the heat and mass transfer mechanisms.
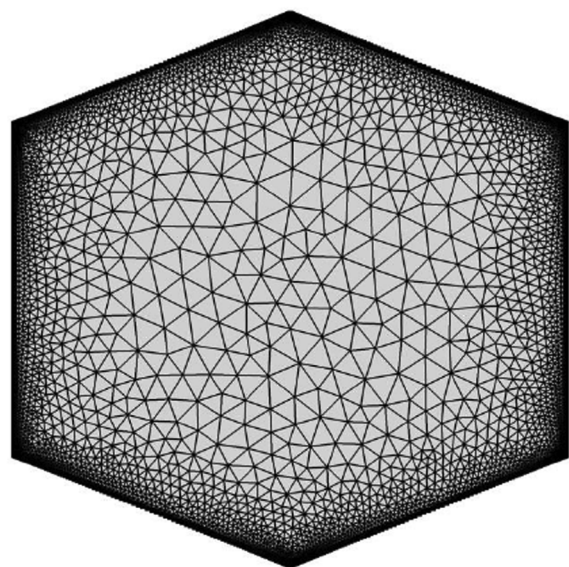

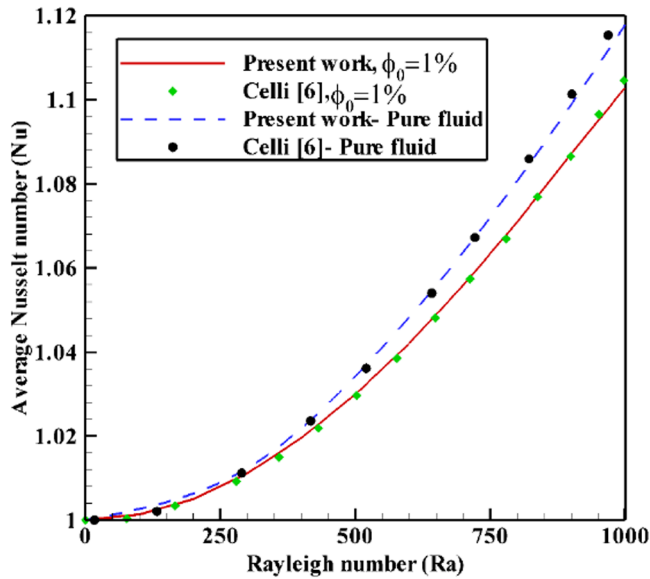**Fig. 2.** The illustration of selected mesh.

Fig. 3. A comparison of average Nusselt number as a function of Rayleigh number in the present and that of Celli [6].
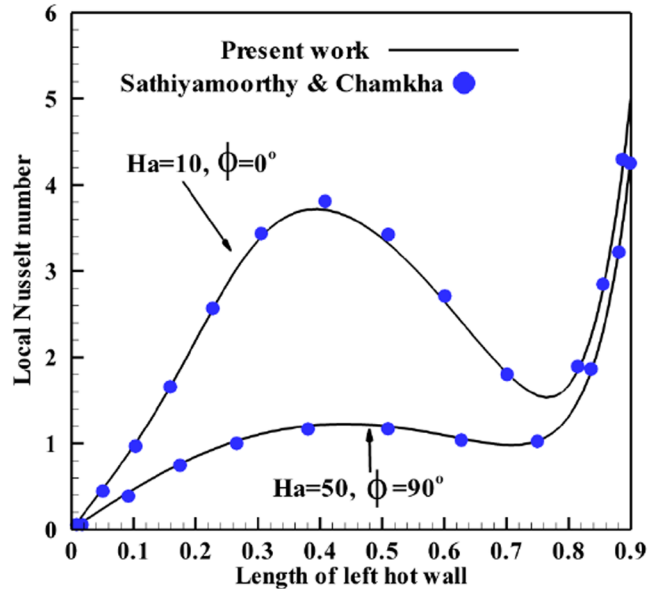

Fig. 4. A comparison of local Nusselt number on the hot wall in the present study and that of Sathiyamoorthy and Chamkha [2].

Table 4
Determining the range and default values for the dimensionless parameter in the present study.

Parameter	Minimum value	Maximum value	Default value
Rayleigh number (Ra)	10^3	10^4	10^4
Dynamic viscosity (N_v)	3	10	7
Thermal conductivity (N_c)	3	10	7
Buoyancy ratio (N_r)	1	20	5
Brownian motion (N_b)	5×10^{-7}	5×10^{-6}	10^{-6}
Thermophoresis motion (N_t)	10^{-7}	10^{-6}	5×10^{-7}
Hartmann number (Ha)	5	10	5
Magnetic number (Mnf)	$5 \times 10^{+2}$	10^{+3}	$5 \times 10^{+2}$

By positioning the magnetic source in situations 3 and 4 (the top areas of the enclosure), the presence of the nanofluid in the top areas of the enclosure is insignificant. Also, space and freedom degree of the

Table 5
Assessment of heat and mass transfer rate, and average velocity for different formations of magnetic source.

Case	Position of the local field	Average Nusselt number(Nu_{Avg})	Average Sherwood number(Sh_{Avg})	average velocity(V)
1		1.6327	0.7133	6.4295
2		1.7546	0.7665	5.2391
3		0.7772	0.3406	8.8253
4		1.1000	0.4807	5.6736

nanofluid motion is greatly deteriorated by reducing the thermal and mass gradients of the nanofluid. Therefore, the velocity of the trapped nanofluid increased in the bottom areas of the enclosure. However, positioning a magnetic source in the vicinity of the tilted bottom sides means that the situations 1 and 2 cause the uniform distribution of the nanofluid in a larger space than the situations 3 and 4 in the hexagonal enclosure, which results in enhancing the heat and mass transfer rate and reducing the average velocity of nanofluid. It is worth noting that the rate of reinforcement of heat and mass transfer in the positions 1 and 2 is even more, compared to the conditions where no magnetic field is located beside the enclosure (Table 4). Accordingly, the presence of a magnetic source in situation 2 is more important than other situations.

Fig. 5 displays the contours of average Nusselt and Sherwood numbers for two values of Rayleigh numbers, which are equal to 10^{+3} and 10^{+4} in terms of the effects of magnetic (Mnf) and Hartmann Numbers (Ha). As shown in Fig. 4, an increase in the Rayleigh number improves heat and mass transfer rate. Further, a decrease in the Hartmann Number and the magnetic number leads to an increase in the heat and mass transfer rates. Consequently, the contour in the right-bottom corner has the maximum value of average Nusselt and Sherwood Numbers. However, the average Nusselt number for the two above Rayleigh numbers are 0.9000 and 1.5758, respectively, when no magnetic field is used around the enclosure. On the other hand, the values of the average Sherwood number for the same two Rayleigh Numbers are 0.3931 and, 0.6884, respectively. Hence, regarding all of the selected values of Magnetic and Hartmann Numbers in the two Rayleigh numbers, there is always an improvement in heat and mass transfer rate with respect to the conditions in the absence of local magnetic field. However, an increase in the Hartmann Number shifts the average Nusselt and Sherwood Numbers for the conditions in the absence of local magnetic field, while an increase in the Magnetic number with more improvement of the heat and mass transfer mechanisms represents the advantage of the presence of a local magnetic field around the enclosure (situation 2).

In general, the Lorentz force and Joule heating phenomenon in the nature of the Hartmann number, as well as the Kelvin force and
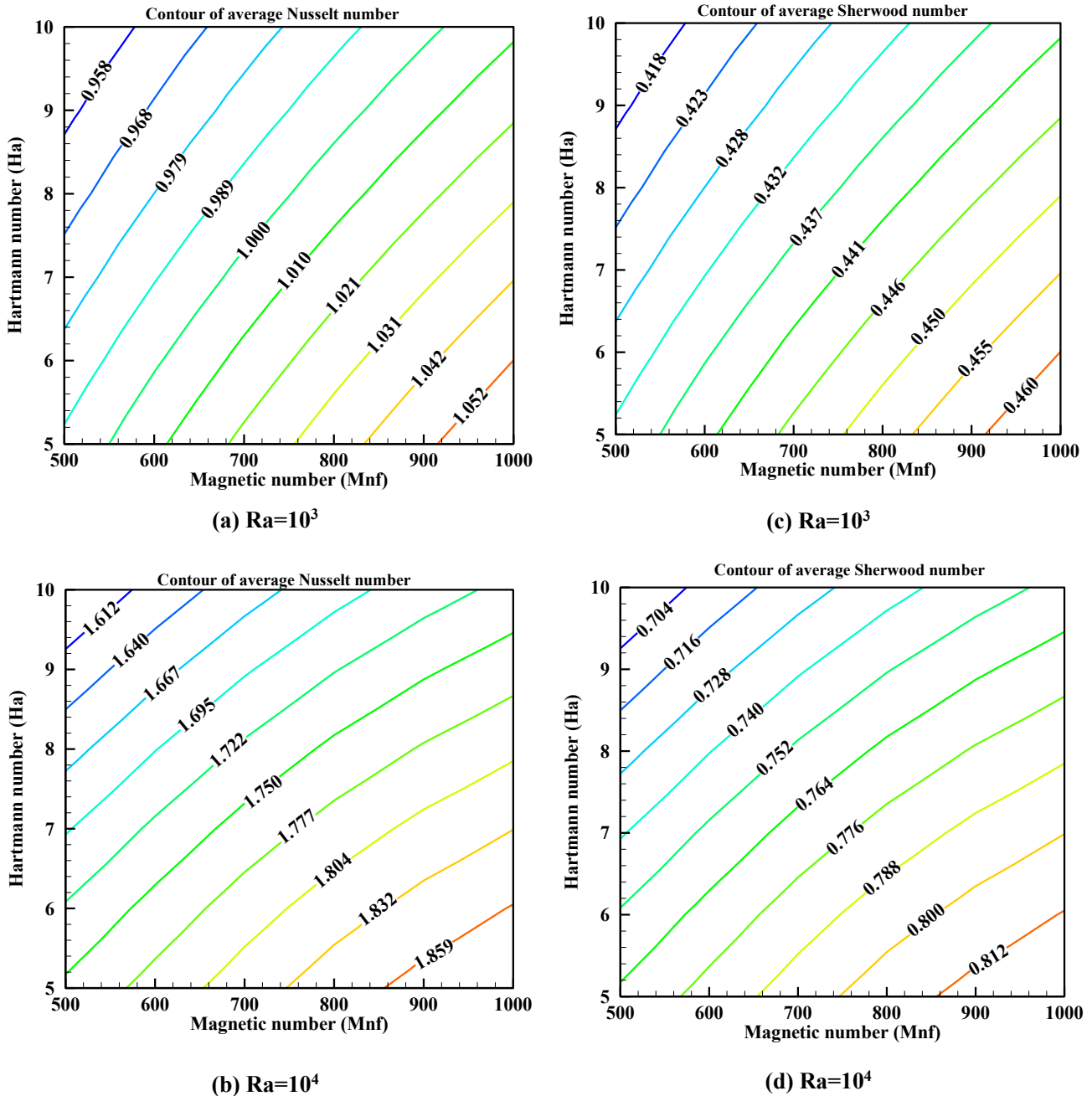
(a) Ra=10³

(c) Ra=10³

(b) Ra=10⁴

(d) Ra=10⁴

Fig. 5. The contours of average Nusselt number in (a) $Ra = 10^3$, (b) $Ra = 10^4$ and contours of average Sherwood number in (c) $Ra = 10^3$, (d) $Ra = 10^4$ for different values of magnetic and Hartmann Numbers.

Magneto-Caloric phenomenon in the format of the magnetic number result in creating some problems. An increase in the interaction between the magnetic and electric fields (Lorentz force) and the conversion rate of electrical energy to heat (Joule Heating effects) lead to a reduction in the heat and mass transfer rate. However, an increase in the generated force by electromagnetic stress (Kelvin force) and the adiabatic cooling (Magneto-Caloric phenomenon) result in increasing the values of average Nusselt and Sherwood numbers inside a hexagonal enclosure. The observed reduction of heat transfer, Fig. 5, due to the increase of Hartmann number was also reported in [21–23] for a single phase model of nanofluids. However, as the utilized models in [21–23] are single phase models, the effect of Hartmann number on the nanoparticles distribution and average Sherwood number was unclear.

Fig. 6a and 6b illustrate the effects of Hartmann (*Ha*) and Magnetic (*Mnf*) numbers on the contours of isotherm against the absence of a

local magnetic field, respectively. As shown in Fig. 6a, isotherm lines are considerably trended toward the central areas of the enclosure, and they are receded from hot and cold walls by increasing the Hartmann number from the default value of 5–10. Fig. 6b shows the improvement of the thermal gradients proportional to an increase in the Magnetic number from the default value of 500 to 1000 so that the isotherm lines can become closer to the vertical side walls. It is worth noting that a decrease and increase in thermal gradients by Hartmann and magnetic numbers are demonstrated in Fig. 6b.

Fig. 7a and b display the streamlines for variations of Hartmann (*Ha*) and magnetic numbers (*Mnf*) inside the enclosure. As shown, the presence of a local magnetic field in situation 2 leads to a different flow formation than the absence of a local magnetic field. Also, the deformation of the nanofluid flow increases by increasing both of these non-dimensional numbers on the right and center of the enclosure.
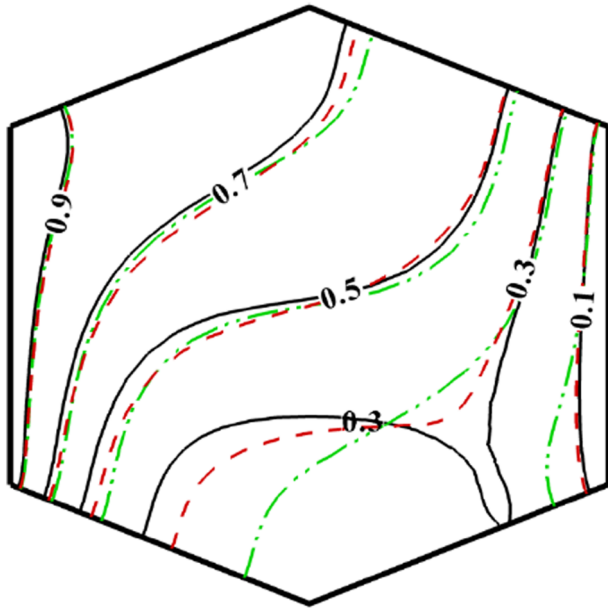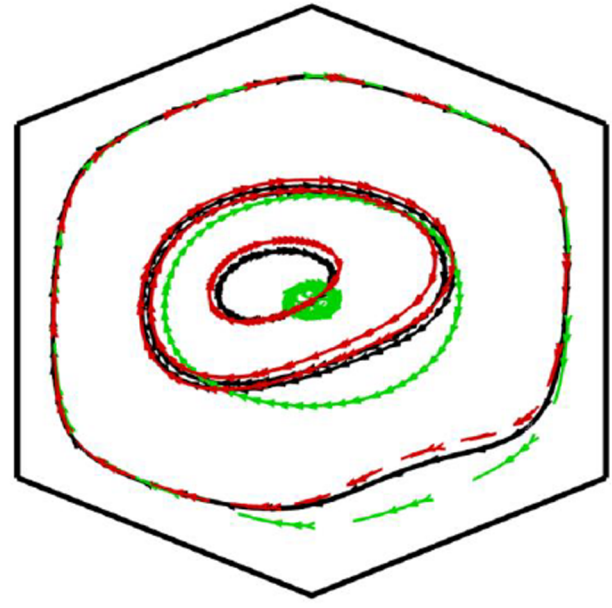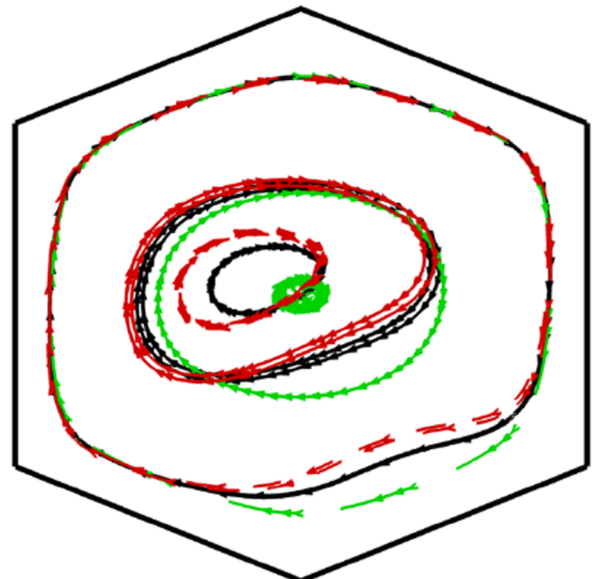
(a)
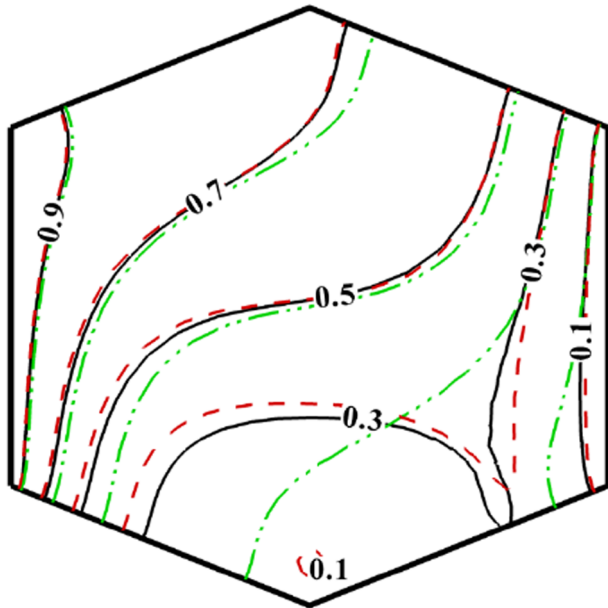
(b)

Fig. 6. Evaluation of isotherm lines for (a) increasing the Hartmann number from the default value 5 (Black continuous lines) to 10 (Red dashed lines), and (b) raising the magnetic number from the default value 500 (Black Continuous lines) to 1000 (Red dashed lines), against the absence of a local magnetic field (Two green point-dashed lines). (For interpretation of the references to colour in this figure legend, the reader is referred to the web version of this article.)

Fig. 7. Evaluation of the streamlines for (a) increasing the Hartmann number from the default value 5 (Black continuous lines) to 10 (Red dashed lines), and (b) increasing the magnetic number from the default value 500 (Black continuous lines) to 1000 (Red dashed lines) against the absence of a local magnetic field (Green long dashed lines). (For interpretation of the references to colour in this figure legend, the reader is referred to the web version of this article.)

However, the deformation of the nanofluid flow due to the increase in the magnetic number, especially in the center of the enclosure, is more tangible than its variation under the influence of increasing in Hartmann number. In other words, the type of changing the pattern of nanofluid flow by magnetic number is different from Hartmann number because increasing the magnetic number gives a positive direction to

the nanofluid flow pattern by improving the heat and mass transfer ratio. Instead, increasing the Hartmann number, along with weakening the heat and mass transfer rate, is known as a disturbing factor in the nanofluid flow circulation.

As it was already mentioned, two non-dimensional parameters
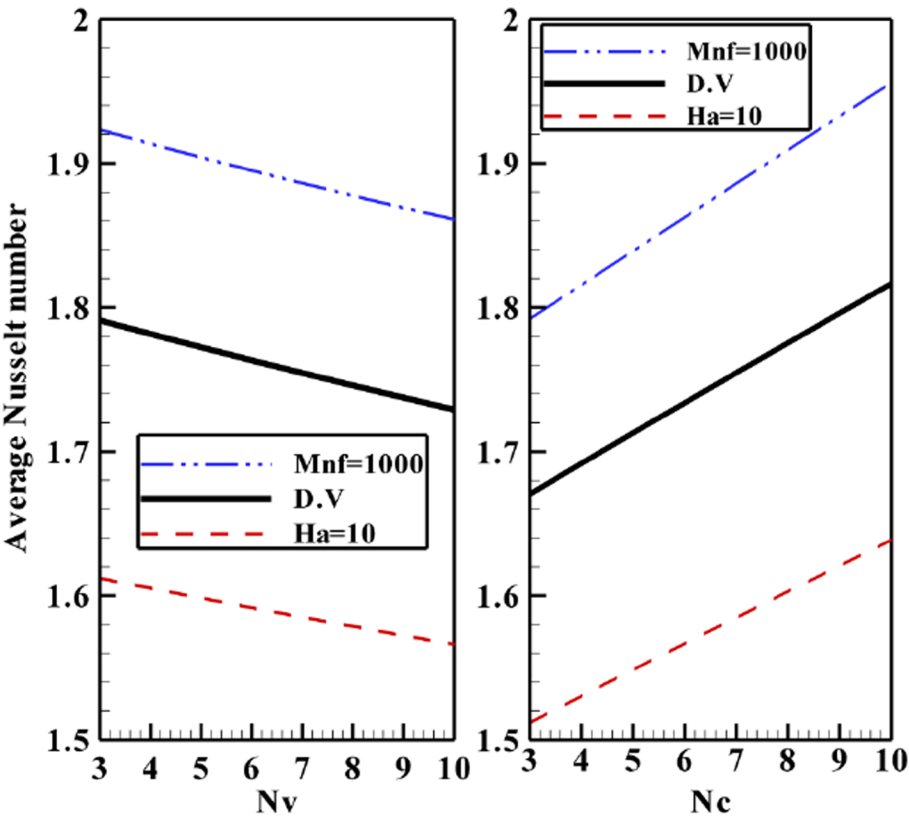
(a)
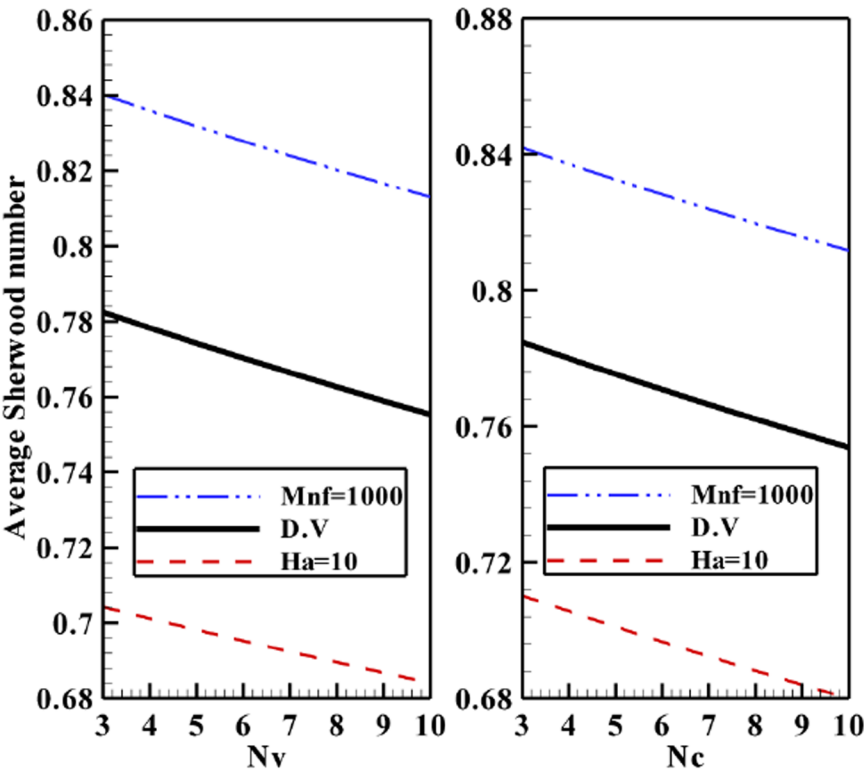
(b)

(caption on next page)

Fig. 8. Effect of dynamic viscosity parameters (left-hand side) and thermal conductivity coefficient (right-hand side) on (a) average Nusselt number and (b) the average Sherwood number in different values of magnetic and Hartmann numbers.

including dynamic viscosity (Nv) and thermal conductivity (Nc) in the nanofluid depend on the shape, size, and type of the nanoparticles, as well as the type of base fluid and fluid operating temperature. Each nanofluid has a constant and exclusive value of the dynamic viscosity and thermal conductivity parameters. For example, Water-TiO$_2$ nanofluid with spherical nanoparticles and a diameter of 21 nm in the ambient temperature (25 °C) has dynamic viscosity and thermal conductivity of 7.65 and 3.87, respectively. Hence, the value of the heat and mass transfer for a range of various nanofluids is evaluated in the presence of the local magnetic field as shown in Fig. 8. The obtained

(a)

(b)

Fig. 9. (a) the average Nusselt number, and (b) the average Sherwood number as a function of Brownian dispersion parameters (Left-hand side) and the thermophoresis dispersion parameter (right-hand side) in different values of magnetic and Hartmann numbers.

curves were presented for default values (Black continues curve) by increasing Hartmann Number (Red dashed curve), and the magnetic number (Blue two points curve). As displayed in Fig. 8, an increase in magnetic and Hartmann numbers for the curve of the default values results in weakening and strengthening the heat and mass transfer, respectively, as illustrated in Fig. 5.

As shown in Fig. 8a, an increase in the dynamic viscosity and thermal conductivity parameters results in decreasing and increasing in the average Nusselt number, respectively. Besides, the amplification of the dynamic viscosity parameter leads to a reduction in heat transfer by weakening the convection heat transfer mechanisms, while the enhancement of the thermal conductivity parameter increases the thermal conductivity of the nanofluid, and accordingly an improvement in the heat transfer rate. On the other hand, as shown in Fig. 8b, increasing the dynamic viscosity parameter weakens the mass transfer rate. The increase in thermal conductivity enhances the heat transfer rate. These outcomes are in agreement with the literature results [1] for single-phase flow and heat transfer of nanofluids in a cavity.

Further, an increase in the dynamic viscosity parameter weakens convection heat transfer mechanism and deteriorates the mass transfer mechanism, which results in decreasing the nanoparticle concentration gradient in the vicinity of the hot wall. In other words, a more viscous nanofluid has less heat and mass capability than a nanofluid with lower viscosity.

As displayed in Fig. 8b, an improvement in the thermal conductivity parameter by decreasing the surface temperature gradient provides more uniform distribution inside the enclosure. The milder and uniform boundary layers appear inside the enclosure, especially in the vicinity of the walls. Hence, the nanoparticle concentration gradient decreases in the vicinity of the hot wall for a nanofluid with a high thermal conductivity parameter, compared to another nanofluid with a low thermal conductivity parameter.

Fig. 9 demonstrated the average Nusselt and Sherwood numbers as a function of Brownian (N_b) and thermophoresis (N_t) dispersion parameters, respectively. Further, the three selected curves in Fig. 8 are evaluated in Fig. 9, which indicates a slight increase and decrease in the average Nusselt number by enhancing the Brownian and thermophoresis dispersion parameters, respectively. Furthermore, an increase in the Brownian dispersion parameter at a constant value for the thermophoresis dispersion parameter increases the probability of nanoparticles presence with various temperatures in the vicinity of hot and cold walls by enhancing the random motion of nanoparticles inside the hexagonal enclosure. As a result, more thermal gradients are created inside the enclosure. Instead, the transfer rate of each nanoparticle between the cold and hot walls increases by the rise of the thermophoresis dispersion parameter in a constant value for the Brownian dispersion parameter. By considering the Eulerian view in the present study, the short-term presence of nanoparticles in the vicinity of the vertical walls, and accordingly the reduction of the opportunity for heat exchange between the walls and the nanofluid are expectable. The trend of the results is in agreement with the literature results of [27].

Besides, a significant decrease and increase are observed in the average Sherwood number through increasing Brownian and Thermophoresis dispersion parameters, respectively (Fig. 9b). As shown, all three curves experienced considerable changes, despite having a low distance to the others. Further, the effective rate of Brownian and thermophoresis dispersion parameters on the mass transfer relative to the given values is more inclement for the Ferrohydromagnetic and Magneto-hydrodynamic parameters. As it was already mentioned, the enhancement of the Brownian dispersion parameter increases random motions of nanoparticles inside the enclosure, leading to a more uniform distribution of nanoparticles. Hence, fewer
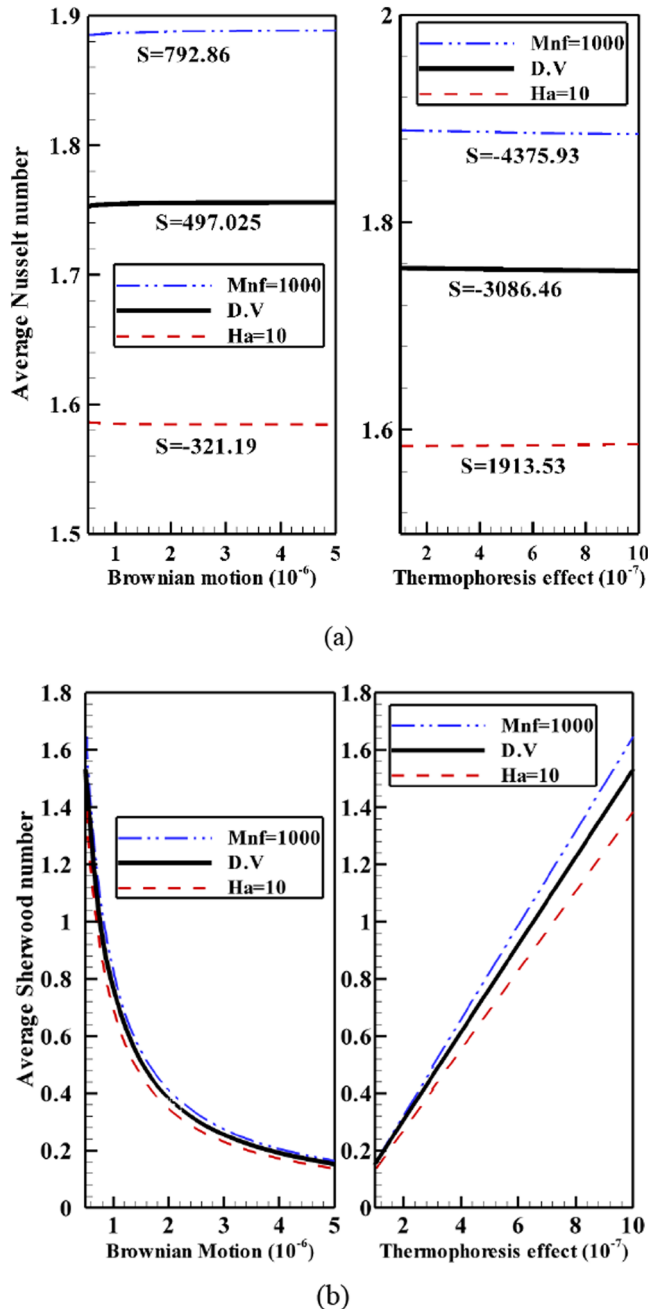
Table 6

Effect of Buoyancy ratio parameter (*Nr*) on the Average Nusselt (*Nu_{avg}*), and Average Sherwood (*Sh_{avg}*) numbers in three different states (*Mnf* = 1000, D.V., and *Ha* = 10).

	Nr				
	1	5	10	15	20
Nu_{avg}					
Mnf = 1000	1.8881	1.8814	1.8696	1.8574	1.8412
D.V.	1.7556	1.7542	1.7524	1.7505	1.7487
Ha = 10	1.5839	1.5830	1.5817	1.5804	1.5787
Sh_{avg}					
Mnf = 1000	0.8257	0.8228	0.8177	0.8117	0.8046
D.V.	0.7678	0.7672	0.7664	0.7656	0.7648
Ha = 10	0.6927	0.6923	0.6917	0.6912	0.6904

concentration gradients are formed about the hot wall. However, an increase in the Thermophoresis dispersion parameter causes a faster exchange of nanoparticles between lateral vertical walls. Thus, the concentration gradient of nanoparticles significantly increased in the vicinity of these walls. Furthermore, the obtained patterns for the Sherwood Number are justified by using the boundary conditions of nanoparticle non-permeability in the vicinity of cold and hot walls. The direct and inverse relationship between the Sherwood number and the thermophoresis and Brownian dispersion parameters can confirm the provided patterns for this non-dimensional number.

In Fig. 9(a) the slope (*S*) for each of the curves is calculated following the method of Shah et al. [39]. The value of *S* is written below each curve of Fig. 9(a). Considering review results of Animasaun et al. [40], the slope of average Nusselt number in the case of Ha = 10 is in agreement with the studies of Haddad et al. [41] and Khan and Pop [28]. In the case of *Mnf* = 1000, the slope is in agreement with the study of Shateyi [42]. Considering the thermophoresis effect, the trend of the results is in agreement with the works of Behseresht et al. [8].

Table. 6 explains the effect of the Buoyancy ratio parameter (*Nr*) on the average Nusselt and Sherwood numbers. The concept of the Buoyancy ratio parameter is summarized in the volume fraction of the nanoparticles. Based on the results, more nanoparticles are sediment when more of them are heavier. However, it is expected that increasing the volume fraction of the nanoparticles decreases the heat and mass transfer rate. Also, the values of three default states, *Mnf* = 1000, D.V. (Default Value of parameters), and *Ha* = 10, are fixed although each has a different decreasing slope by increasing the volume fraction of nanoparticles so that the row related to high Magnetic number can become more sensitive than getting the volume fraction of nanoparticles. However, the row related to high Hartmann number has not considerable reaction than getting the volume fraction of nanoparticles. It seems that more reduction occurs in the heat and mass transfer rate in the face of increasing the volume fraction of nanoparticles when Kelvin force and magneto-caloric phenomenon have a high value (*Mnf* = 1000). However, an increase in Lorentz force and Joule Heating phenomenon (*Ha* = 10) shows that an increase in the volume fraction of nanoparticles results in decreasing heat and mass transfer with a very low slope.

6. Conclusion

In the present study, the mixed convection heat and mass transfer of various nanofluids were evaluated inside a hexagonal enclosure in the presence of a magnetic source. The governing equations and related boundary conditions were transferred into their non-dimensional form and were solved by finite element computational method (FEM). The obtained results were analyzed in the form of non-dimensional numbers/parameters, contours of isotherm, and streamlines. The results of the present study are compared with the literature results in the case of

MHD flow and nanofluid flow and found in good agreement. The trend of the results in the case of two-phase flow of nanofluid is also in agreement with the literature results considering the method of slope linear regression. The most important results are as follows:

I. The location of the magnetic source is effective on the average Nusselt (*Nu*) and Sherwood (*Sh*) numbers. In other words, heat and mass transfer increases if the magnetic source is placed in a situation, which is consistent with the nanofluid flow. However, heat and mass transfer rate are deteriorated if a magnetic source suppresses the natural circulation of nanofluid due to a particular situation.

II. Increasing magnetic number (*Mnf*) by augmenting Kelvin force and Magneto-caloric effect results in increased heat and mass transfer rate.

III. Increasing Lorentz force and Joule-heating phenomenon in the form of Hartmann number (*Ha*) leads to a decrease in the rate of heat and mass transfer.

IV. Average Nusselt number decreases and increases by increasing dynamic viscosity (*Nv*) and thermal conductivity (*Nc*) parameters, respectively, although the average Sherwood number is weakened by increasing the two mentioned parameters.

V. Variations of Brownian (*N_b*) and thermophoresis (*N_t*) parameters insignificantly affect the average Nusselt number of nanofluid while changing Brownian and thermophoresis parameters play a significant role in the mass transfer. These two parameters decrease and increase mass transfer, respectively.

VI. Increasing the volume fraction of nanoparticles debilitates heat and mass transfer rate, which is significant for the high value of the magnetic number and subtle for a high value of Hartmann number.

The outcomes of the present stud show that MHD and FHD effects can change the migration and distribution of nanoparticles in the enclosure. As the magnetic field is capable of altering the flow and heat transfer of nanofluids in natural convection, it can be utilized as a control variable to adjust the heat transfer in an industrial process.

Moreover, the nanoparticles by their migration can transfer a small amount of energy in the nanofluid. However, the thermophysical properties of the nanofluid can notably change by the change of the nanoparticles' concentration. As the migration of nanoparticles changes the local concentration of nanoparticles, the consideration of the variation of the local properties of the nanofluid by the migration of nanoparticles can be subject of future studies.

Appendix A. Supplementary data

Supplementary data to this article can be found online at https://doi.org/10.1016/j.jmmm.2019.166024.

References

[1] M. Sabour, M. Ghalambaz, A. Chamkha, Natural convection of nanofluids in a cavity: criteria for enhancement of nanofluids, Int. J. Numer. Meth. Heat Fluid Flow 27 (2017) 1504–1534.

[2] M. Sathiyamoorthy, A.J. Chamkha, Natural convection flow under magnetic field in a square cavity for uniformly (or) linearly heated adjacent walls, Int. J. Numer. Meth. Heat Fluid Flow 22 (2012) 677–698.

[3] M. Sheikholeslami, D.D. Ganji, Ferrohydrodynamic and magnetohydrodynamic effects on ferrofluid flow and convective heat transfer, Energy 75 (2014) 400–410.

[4] J. Buongiorno, Convective transport in nanofluids, J. Heat Transfer 128 (2006) 240–250.

[5] J. Buongiorno, D.C. Venerus, N. Prabhat, T. McKrell, J. Townsend, R. Christianson, Y.V. Tolmachev, P. Keblinski, L.-W. Hu, J.L. Alvarado, A benchmark study on the thermal conductivity of nanofluids, J. Appl. Phys. 106 (2009) 094312.

[6] M. Celli, Non-homogeneous model for a side heated square cavity filled with a nanofluid, Int. J. Heat Fluid Flow 44 (2013) 327–335.

[7] A. Wakif, Z. Boulahia, A. Amine, I. Animasaun, M. Afridi, M. Qasimd, R. Sehaqui, Magneto-convection of alumina-water nanofluid within thin horizontal layers using the revised generalized Buongiorno's model, Front. Heat Mass Transfer (FHMT) 12 (2018).

[8] A. Behseresht, A. Noghrehabadi, M. Ghalambaz, Natural-convection heat and mass transfer from a vertical cone in porous media filled with nanofluids using the practical ranges of nanofluids thermo-physical properties, Chem. Eng. Res. Des. 92 (2014) 447–452.

[9] O. Mahian, L. Kolsi, M. Amani, P. Estellé, G. Ahmadi, C. Kleinstreuer, J.S. Marshall, M. Siavashi, R.A. Taylor, H. Niazmand, Recent advances in modeling and simulation of nanofluid flows-part I: fundamental and theory, Phys. Rep. (2018).

[10] O. Mahian, L. Kolsi, M. Amani, P. Estellé, G. Ahmadi, C. Kleinstreuer, J.S. Marshall, R.A. Taylor, E. Abu-Nada, S. Rashidi, Recent advances in modeling and simulation of nanofluid flows-part II: applications, Phys. Rep. (2018).

[11] A. Hajizadeh, N.A. Shah, S.I.A. Shah, I. Animasaun, M. Rahimi-Gorji, I.M. Alarifi, Free convection flow of nanofluids between two vertical plates with damped thermal flux, J. Mol. Liq. 110964 (2019).

[12] I. Animasaun, O. Koriko, K. Adegbie, H. Babatunde, R. Ibraheem, N. Sandeep, B. Mahanthesh, Comparative analysis between 36 nm and 47 nm alumina-water nanofluid flows in the presence of Hall effect, J. Therm. Anal. Calorim. 135 (2019) 873–886.

[13] H.T. Basha, I. Animasaun, O. Makinde, R. Sivaraj, Effect of electro-magnetohydrodynamic on chemically reacting nanofluid flow over a cone and plate, Applied Mathematics and Scientific Computing, Springer, 2019, pp. 99–107.

[14] J.M. Coey, Magnetism and Magnetic Materials, Cambridge University Press, 2010.

[15] Y. Haik, V. Pai, C.-J. Chen, Development of magnetic device for cell separation, J. Magn. Magn. Mater. 194 (1999) 254–261.

[16] E. Tzirtzilakis, M. Xenos, Biomagnetic fluid flow in a driven cavity, Meccanica 48 (2013) 187–200.

[17] N. Al-Najem, K. Khanafer, M. El-Refaee, Numerical study of laminar natural convection in tilted enclosure with transverse magnetic field, Int. J. Numer. Meth. Heat Fluid Flow 8 (1998) 651–672.

[18] F. Selimefendigil, H.F. Öztop, A.J. Chamkha, MHD mixed convection and entropy generation of nanofluid filled lid driven cavity under the influence of inclined magnetic fields imposed to its upper and lower diagonal triangular domains, J. Magn. Magn. Mater. 406 (2016) 266–281.

[19] M. Ghalambaz, A. Doostanidezfuli, H. Zargartalebi, A.J. Chamkha, MHD phase change heat transfer in an inclined enclosure: effect of a magnetic field and cavity inclination, Numer. Heat Transfer, Part A: Appl. 71 (2017) 91–109.

[20] A. Chamkha, M. Ismael, A. Kasaeipoor, T. Armaghani, Entropy generation and natural convection of CuO-water nanofluid in C-shaped cavity under magnetic field, Entropy 18 (2016) 50.

[21] Y. Ma, R. Mohebbi, M. Rashidi, Z. Yang, M.A. Sheremet, Numerical study of MHD nanofluid natural convection in a baffled U-shaped enclosure, Int. J. Heat Mass Transf. 130 (2019) 123–134.

[22] A. Dogonchi, M.A. Sheremet, I. Pop, D. Ganji, MHD natural convection of Cu/H2O nanofluid in a horizontal semi-cylinder with a local triangular heater, Int. J. Numer. Meth. Heat Fluid Flow 28 (2018) 2979–2996.

[23] C. Sivaraj, M. Sheremet, MHD natural convection and entropy generation of ferrofluids in a cavity with a non-uniformly heated horizontal plate, Int. J. Mech. Sci. 149 (2018) 326–337.

[24] M. Sheikholeslami, K. Vajravelu, M.M. Rashidi, Forced convection heat transfer in a semi annulus under the influence of a variable magnetic field, Int. J. Heat Mass Transf. 92 (2016) 339–348.

[25] H. Aminfar, M. Mohammadpourfard, F. Mohseni, Two-phase mixture model simulation of the hydro-thermal behavior of an electrical conductive ferrofluid in the presence of magnetic fields, J. Magn. Magn. Mater. 324 (2012) 830–842.

[26] M.R. Dibavar, M. Mohammadpourfard, F. Mohseni, S.Z. Heris, Numerical study on the effect of non-uniform magnetic fields on melting and solidification characteristics of NEPCMs in an annulus enclosure, Energy Convers. Manage. 171 (2018) 879–889.

[27] M.A. Sheremet, I. Pop, Conjugate natural convection in a square porous cavity filled by a nanofluid using Buongiorno's mathematical model, Int. J. Heat Mass Transf. 79 (2014) 137–145.

[28] W. Khan, I. Pop, Boundary-layer flow of a nanofluid past a stretching sheet, Int. J. Heat Mass Transf. 53 (2010) 2477–2483.

[29] I. Hashim, A. Alsabery, M. Sheremet, A. Chamkha, Numerical investigation of natural convection of Al2O3-water nanofluid in a wavy cavity with conductive inner block using Buongiorno's two-phase model, Adv. Powder Technol. 30 (2019) 399–414.

[30] M. Astanina, E. Abu-Nada, M. Sheremet, Combined effects of thermophoresis, brownian motion, and nanofluid variable properties on CuO-water nanofluid natural convection in a partially heated square cavity, J. Heat Transfer 140 (2018) 082401.

[31] C.-J. Ho, M. Chen, Z. Li, Numerical simulation of natural convection of nanofluid in a square enclosure: effects due to uncertainties of viscosity and thermal conductivity, Int. J. Heat Mass Transf. 51 (2008) 4506–4516.

[32] O. Jefimenko, Electricity and Magnetism, Appleton-Century-Crofts, New York, 1966.

[33] M. Sabour, M. Ghalambaz, Natural convection in a triangular cavity filled with a nanofluid-saturated porous medium using three heat equation model, Can. J. Phys. 94 (2016) 604–615.

[34] A. Zaraki, M. Ghalambaz, A.J. Chamkha, M. Ghalambaz, D. De Rossi, Theoretical analysis of natural convection boundary layer heat and mass transfer of nanofluids: effects of size, shape and type of nanoparticles, type of base fluid and working temperature, Adv. Powder Technol. 26 (2015) 935–946.

[35] M. Ghalambaz, A. Behseresht, J. Behseresht, A. Chamkha, Effects of nanoparticles diameter and concentration on natural convection of the Al2O3-water nanofluids considering variable thermal conductivity around a vertical cone in porous media, Adv. Powder Technol. 26 (2015) 224–235.

[36] D. Venerus, J. Buongiorno, R. Christianson, J. Townsend, I.C. Bang, G. Chen, S.J. Chung, M. Chyu, H. Chen, Y. Ding, Viscosity measurements on colloidal dispersions (nanofluids) for heat transfer applications, Appl. Rheol. 20 (2010).

[37] M.H. Souli, D.J. Benson, Arbitrary Lagrangian Eulerian and Fluid-Structure Interaction: Numerical Simulation, John Wiley & Sons, 2013.

[38] R. Codina, G. Houzeaux, H. Coppola-Owen, J. Baiges, The fixed-mesh ALE approach for the numerical approximation of flows in moving domains, J. Comput. Phys. 228 (2009) 1591–1611.

[39] N.A. Shah, I. Animasaun, R. Ibraheem, H. Babatunde, N. Sandeep, I. Pop, Scrutinization of the effects of Grashof number on the flow of different fluids driven by convection over various surfaces, J. Mol. Liq. 249 (2018) 980–990.

[40] I. Animasaun, R. Ibraheem, B. Mahanthesh, H. Babatunde, A meta-analysis on the effects of haphazard motion of tiny/nano-sized particles on the dynamics and other physical properties of some fluids, Chin. J. Phys. (2019).

[41] Z. Haddad, E. Abu-Nada, H.F. Oztop, A. Mataoui, Natural convection in nanofluids: are the thermophoresis and Brownian motion effects significant in nanofluid heat transfer enhancement? Int. J. Therm. Sci. 57 (2012) 152–162.

[42] S. Shateyi, Numerical analysis of three-dimensional MHD nanofluid flow over a stretching sheet with convective boundary conditions through a porous medium, Nanofluid Heat Mass Trans. Eng. Problems (2017).